Fracture Mechanics of Concrete Structures, de Borst et al (eds) © 2001 Swets & Zeitlinger, Lisse, ISBN 90 2651 825 0

Equivalent Localization Element for Crack Band Model and as Alternative to Elements with Embedded Discontinuities

Zdeněk P. Bažant
Walter P. Murphy Professor of Civil Engineering and Material Science, Northwestern University, Evanston, Illinois 60208, USA

Jan Cervenka & Martin Wierer
Cervenka Consulting, Prague, Czech Republic

ABSTRACT: The paper presents a novel method making it possible to apply complex material models, such as the microplane model, in finite element calculations with variable finite element sizes, and with element sizes larger than the material characteristic length.

1 INTRODUCTION

Brittle materials such as concrete, rock or masonry exhibit strain-softening behavior in the post-peak, both in tension and in compression. In numerical modeling by the finite element method, the first consequence of the strain softening is the dependence of results on the finite element sizes. If a material model is defined using solely stress-strain relations, the energy dissipated during brittle failure will depend on the finite element sizes in the critical regions. In the limit of a vanishing element size, this can result in a zero energy dissipation during failure, which is physically impossible.

The second consequence of the strain softening is that the underlying mathematical formulation becomes ill-posed. In non-linear numerical solutions by the finite element method, which usually involve some sort of an iterative algorithm, this phenomenon gets manifested by oscillatory convergence or even the failure to reach prescribed convergence limits. This consequence produces a dependence on the orientation of the finite element mesh.

One remedy for the first consequence of strain softening, i.e. the mesh size dependence, is the crack band model of Bažant and Oh (1983). The basic idea of this model is to modify the material parameters such that the energy dissipated by large and small elements be identical.

Non-local approaches were introduced as a remedy to the mesh orientation bias when sufficiently small elements can be used.

The crack band model is currently used in commercial finite element codes only in combination with relatively simple material models. The new and more advanced material models are usually developed within the framework of the non-local approach. These new models can usually simulate rather complex loading scenarios, but their application to practical engineering problems is difficult, due to the requirement that the finite element size in the failure zone should be significantly less than the characteristic length of the material. For real-life structures, this requirement leads to a very large number of elements, although this can be mitigated by some elaborate adaptive scheme. The crack band model cannot be applied in its current form, since for such material models it is not easy to identify which material parameters should be adjusted according to the element size to ensure correct energy dissipation. A typical such material model is the microplane model, whose initial version was developed by Bažant (1984). This model contains parameters, which were calibrated for sizes close to the material characteristic length and cannot be easily adjusted.

This paper presents a novel method that makes it possible to apply the microplane model in finite element computations with elements of different sizes, much larger then the material characteristic length. Applicable though the present method is to other material models and other materials, this paper deals only with applications to the microplane model and to concrete. The specific formulation of the microplane by Bažant et. al (2000a, 2000b) is used throughout this paper.

2 CRACK BAND MODEL

In the crack band model, the material parameters are adjusted such that the same amount of energy is dissipated during the failures of a large and a small finite element. This is usually accomplished using the assumption that a single localization zone (i.e., a crack or crack band) develops inside the element. Using this assumption, the crack opening displace-

ment w can be calculated from the fracturing strain ε^f using the crack band size L (width) and the following simple formula:

$$w = L\,\varepsilon^f \tag{1}$$

where L can be determined based on the finite element size projected into the direction of maximum principal strain for the case of tensile cracking and low order finite elements.

3 MICROPLANE MODEL

The basic idea of the microplane model is to abandon constitutive modeling in terms of tensors and their invariants and formulate the stress-strain relation in terms of stress and strain vectors on planes of various orientation in the material, now generally called the microplanes. This idea arose in G.I. Taylor's (1938) pioneering study of hardening plasticity of polycrystalline metals. Proposing the first version of the microplane model, Bažant (1984), in order to model strain-softening, extended or modified Taylor's model in several ways (in detail see Bažant et al. 2000a), of which the main one was the kinematic constraint between the strain tensor and the microplane strain vectors. Since 1984, there have been numerous improvements and variations of the microplane approach. A detailed overview of the history of the microplane model is included in Bažant et. al (2000a, 2000b). This paper also contains the detailed derivations of the microplane model that is used in this work.

In the microplane model, the constitutive equations are formulated on a plane called microplane with an arbitrary orientation characterized by its unit normal n_i. The kinematic contraint means that the normal strain ε_N and shear strains $\varepsilon_M, \varepsilon_L$ on the microplane are calculated as the projections of the macroscopic strain tensor:

$$\varepsilon_N = n_i n_j \varepsilon_{ij},$$

$$\varepsilon_M = \frac{1}{2}\left(m_i n_j + m_j n_i\right)\varepsilon_{ij}, \tag{2}$$

$$\varepsilon_L = \frac{1}{2}\left(l_i n_j + l_j n_i\right)\varepsilon_{ij}$$

where m_i and l_i are chosen orthogonal vectors lying in the microplane and defining the shear strain components. The constitutive relations for the microplane strains and stresses can be generally stated as:

$$\sigma_N(t) = F^t_{\tau=0}\left[\varepsilon_N(\tau), \varepsilon_M(\tau), \varepsilon_L(\tau)\right]$$

$$\sigma_M(t) = G^t_{\tau=0}\left[\varepsilon_N(\tau), \varepsilon_M(\tau), \varepsilon_L(\tau)\right] \tag{3}$$

$$\sigma_L(t) = H^t_{\tau=0}\left[\varepsilon_N(\tau), \varepsilon_M(\tau), \varepsilon_L(\tau)\right]$$

where F, G and H are functionals of the history of the microplane strains in time t. For a detailed derivation of these functionals a reader is referred to

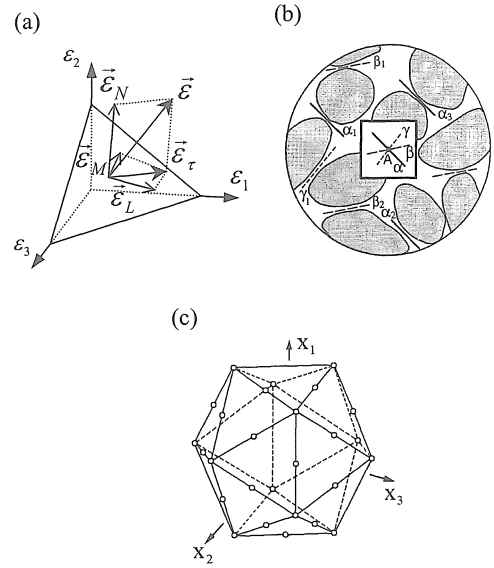

Figure 1. Fundamental concepts of the microplane model

Bažant et. al (2000a, 2000b). The macroscopic stress tensor is obtained by the principle of virtual work that is formulated for a unit hemisphere Ω. After the integration, the following expression for the macroscopic stress tensor is recovered (Bažant et. al 2000a, 2000b):

$$\sigma_{ij} = \frac{3}{2\pi}\int_\Omega s_{ij}\,d\Omega \approx 6\sum_{\mu=1}^{N_m} w_\mu s_{ij}^{(\mu)} \tag{4}$$

$$s_{ij} = \sigma_N n_i n_j + \frac{\sigma_M}{2}\left(m_i n_j + m_j n_i\right) + \frac{\sigma_L}{2}\left(l_i n_j + l_j n_i\right) \tag{5}$$

where the integral is approximated by an optimal Gaussian integration formula for a spherical surface.

The version M4 of the microplane model has been implemented into a commercial finite element code ATENA and will be used in all the examples throughout this paper.

4 ONE-DIMENSIONAL EQUIVALENT ELEMENT

The basic idea of the equivalent localization element is identical to the crack band model approach. This time, however, the material properties and parameters of the softening material model are not modified to account for the different finite element size, but rather the softening material is coupled with an elastic spring in a series arrangement. For a large finite element, the length of the additional elastic spring will be much larger then the size of the localization zone. Thus, after the crack initiation, the energy

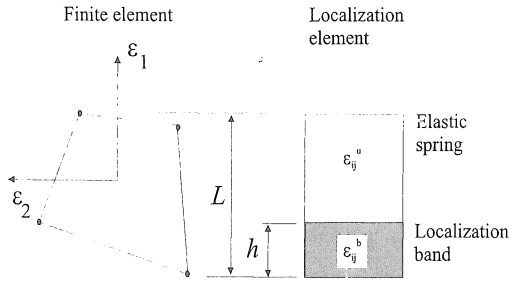

Figure 2. Equivalent localization element

stored in the elastic spring can be readily transferred to the localization zone and dissipated in the softening (i.e. fracturing) process.

Inside each finite element at each integration point, an equivalent localization element is assumed. The localization element represents a serial arrangement of a localization zone which is loading and an elastic zone (spring) which is unloading. The total length of the element is equivalent to the crack band size L (width), and can be determined using the same methods as described in Section 2. The width of the localization zone is given by the characteristic length of the material, or by the size of the test specimen for which the material model used has been calibrated. The direction of the localization element, given by the normal to the localization and elastic zone, should be perpendicular to the plane of failure propagation. An appropriate definition of this direction is significant and not trivial, and it will be discussed later in this paper. For the time being, let us assume that the direction of failure propagation is known. The direction of crack propagation is denoted by local cartesian coordinate subscript 2, and the direction of the localization element by 1.

The strain tensor can be separated into two parts: strains in the elastic spring that are denoted by superscript u, and strains in the localization band with superscript b.

The displacement compatibility condition for the whole length of the equivalent localization element gives the following relationship between the finite element strain vector $\boldsymbol{\varepsilon}$, the strain vector $\boldsymbol{\varepsilon}^u$ in the unloading elastic zone and the strain vector in the localization band $\boldsymbol{\varepsilon}^b$:

$$L\boldsymbol{\varepsilon} = h\boldsymbol{\varepsilon}^b + (L-h)\boldsymbol{\varepsilon}^u \tag{6}$$

where h is the width of the localization band. The components of the strain and stress vectors are assumed to be transformed into a frame defined by directions 1 and 2, and they are arranged in the following manner:

$$\boldsymbol{\varepsilon} = \{\boldsymbol{\xi}, \boldsymbol{\eta}\}^T \text{ and } \boldsymbol{\sigma} = \{\mathbf{s}, \mathbf{t}\}^T \tag{7}$$

where

$$\boldsymbol{\xi} = \{\varepsilon_{11}, 2\varepsilon_{12}, 2\varepsilon_{13}\}^T, \quad \boldsymbol{\eta} = \{\varepsilon_{22}, \varepsilon_{33}, 2\varepsilon_{23}\}^T \tag{8}$$

$$\mathbf{s} = \{\sigma_{11}, \sigma_{12}, \sigma_{13}\}^T, \quad \mathbf{t} = \{\sigma_{22}, \sigma_{33}, \sigma_{23}\}^T \tag{9}$$

Using the foregoing stress and strain vector components, one can define the analogous components of the constitutive matrix and write

$$\boldsymbol{\sigma} = \begin{Bmatrix} \mathbf{s} \\ \mathbf{t} \end{Bmatrix} = \mathbb{D} \begin{Bmatrix} \boldsymbol{\xi} \\ \boldsymbol{\eta} \end{Bmatrix} = \begin{matrix} \mathbb{D}^{ss} & \mathbb{D}^{st} \\ \mathbb{D}^{ts} & \mathbb{D}^{tt} \end{matrix} \begin{Bmatrix} \boldsymbol{\xi} \\ \boldsymbol{\eta} \end{Bmatrix} \tag{10}$$

The localization element is considered only in the direction 1, which is perpendicular to the failure propagation. This implies the following conditions for the components of the strain vectors:

$$L\boldsymbol{\xi} = h\boldsymbol{\xi}^b + (L-h)\boldsymbol{\xi}^u \tag{11}$$

$$\boldsymbol{\eta} = \boldsymbol{\eta}^b = \boldsymbol{\eta}^u \tag{12}$$

and stress vectors:

$$\mathbf{s} = \mathbf{s}^b = \mathbf{s}^u \tag{13}$$

$$\mathbf{t} = \frac{h}{L}\mathbf{t}^b + \frac{L-h}{L}\mathbf{t}^u \tag{14}$$

The equilibrium condition (13) must be satisfied by the stresses in the elastic and localization zones. The stresses in the elastic zone are easily calculated using the elastic constitutive matrix;

$$\mathbf{s}^u = \mathbf{s}^{u0} + \begin{matrix} \mathbb{D}^{ss} & \mathbb{D}^{st} \end{matrix} \begin{Bmatrix} \Delta\boldsymbol{\xi}^u \\ \Delta\boldsymbol{\eta} \end{Bmatrix} \tag{15}$$

$$\mathbf{s}^b = F^s(\boldsymbol{\varepsilon}^{b0}, \Delta\boldsymbol{\varepsilon}^b) \tag{16}$$

The equations (11) to (16) form a system of nonlinear equations which can be solved for instance by the Newton-Raphson iterations as it is described in detail in Cervenka et. al. (2001).

Once the iterative algorithm has satisfied the prescribed convergence criteria, the separation of the total strain tensor into the elastic zone strains and the localization band strain is known. The global stress tensor is then calculated from (13) and (14).

After a close examination of these formulas, it is important to note that stress components on planes parallel to the localization element direction are calculated by summation of the appropriate stress components in the elastic zone and the localization band. This means that the one-dimensional equivalent localization element is suitable only for problems in which the localization causes the increase of only one principal strain component, while the others remain small and within the elastic regime. To alleviate these restrictions, the proposed method will now be extended to a full three-dimensional setting.

5 THE THREE-DIMENSIONAL EQUIVALENT LOCALIZATION ELEMENT

The method proposed in the previous section would be applicable only for cases with pure tension or bending. This constraint can be removed by extending the suggested technique into full 3D with

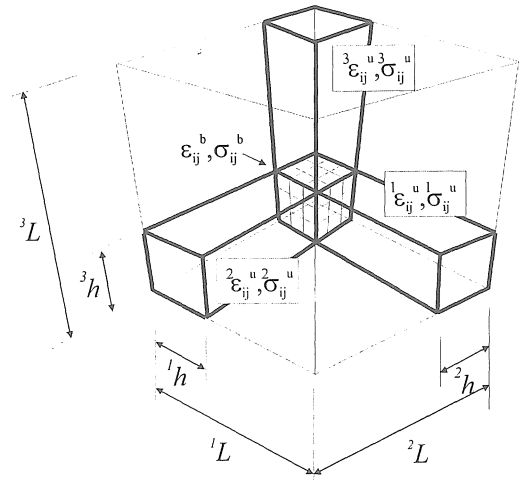

Figure 3. The arrangement of the three-dimensional equivalent localization element.

three localization directions. Arbitrary three perpendicular direction could be used, but it is suitable to use the directions defined by the principal frame of the total macroscopic strain tensor.

The three-dimensional equivalent localization element is constructed in analogy to the one-dimensional case, but this time three serial arrangements of the elastic zone (spring) and localization band are defined. The spring-band systems are perpendicular to each other, and are arranged in parallel to the principal strain directions (Figure 3). In this arrangement of spring-band systems it is possible to identify the following unknown stresses and strains:

$\sigma_{ij}^b, {}^1\sigma_{ij}^u, {}^2\sigma_{ij}^u, {}^3\sigma_{ij}^u$ and $\varepsilon_{ij}^b, {}^1\varepsilon_{ij}^u, {}^2\varepsilon_{ij}^u, {}^3\varepsilon_{ij}^u$

where the superscript b denotes the quantities in the localization band and the superscript u^m defines the quantities in the elastic spring in the direction m. Altogether there are 48 unknown variables. In the subsequent derivations, it is assumed that these stresses and strains are defined in the principal frame of the total macroscopic strain tensor.

The set of available equations for their determination starts with the constitutive formulas for the band and the elastic springs:

$$\sigma_{ij}^b = F(\varepsilon_{ij}^b) \tag{17}$$

$${}^m\sigma_{ij}^u = D_{ijlk}\,{}^m\varepsilon_{kl}^u \quad \text{for } m=1...3 \tag{18}$$

The first formula, (17), represents the evaluation of the non-linear material model, which in our case is the microplane model for concrete. The second equation, (18), is a set of three elastic constitutive formulations for the three linear springs that are involved in the arrangement in Figure 3. This provides the first 24 equations that can be used for the calculation of unknown strains and stresses.

The second set of equations is provided by kinematic constraints on the strain tensors.

$$\varepsilon_{11} = \frac{1}{L^1}\ \varepsilon_{11}^b\,{}^1h + {}^1\varepsilon_{11}^u\left({}^1L - {}^1h\right)$$

$$\varepsilon_{22} = \frac{1}{L^2}\ \varepsilon_{22}^b\,{}^2h + {}^2\varepsilon_{22}^u\left({}^2L - {}^2h\right)$$

$$\varepsilon_{33} = \frac{1}{L^3}\ \varepsilon_{33}^b\,{}^3h + {}^3\varepsilon_{33}^u\left({}^3L - {}^3h\right)$$

$$\varepsilon_{12} = \frac{1}{2}\left\{\frac{1}{{}^1L}\ \varepsilon_{12}^b\,{}^1h + {}^1\varepsilon_{12}^u\left({}^1L - {}^1h\right) + \frac{1}{{}^2L}\ \varepsilon_{12}^b\,{}^2h + {}^2\varepsilon_{12}^u\left({}^2L - {}^2h\right)\right\}$$

$$\varepsilon_{23} = \frac{1}{2}\left\{\frac{1}{{}^2L}\ \varepsilon_{23}^b\,{}^2h + {}^2\varepsilon_{23}^u\left({}^2L - {}^2h\right) + \frac{1}{{}^3L}\ \varepsilon_{23}^b\,{}^3h + {}^3\varepsilon_{23}^u\left({}^3L - {}^3h\right)\right\}$$

$$\varepsilon_{13} = \frac{1}{2}\left\{\frac{1}{{}^1L}\ \varepsilon_{13}^b\,{}^1h + {}^1\varepsilon_{13}^u\left({}^1L - {}^1h\right) + \frac{1}{{}^3L}\ \varepsilon_{13}^b\,{}^3h + {}^3\varepsilon_{13}^u\left({}^3L - {}^3h\right)\right\} \tag{19}$$

These 6 additional equations can be written symbolically as:

$$\varepsilon_{ij} = \frac{1}{2}\left\{\frac{1}{{}^iL}\ \varepsilon_{ij}^b\,{}^ih + {}^i\varepsilon_{ij}^u\left({}^iL - {}^ih\right) + \frac{1}{{}^jL}\ \varepsilon_{ij}^b\,{}^jh + {}^j\varepsilon_{ij}^u\left({}^jL - {}^jh\right)\right\} \tag{20}$$

The next set of equations is obtained by enforcing equilibrium in each direction between the corresponding stress components in the elastic spring and in the localization band. For each direction m, the following condition must be satisfied:

$$\sigma_{ij}^b\,{}^me_j = {}^m\sigma_{ij}^u\,{}^me_j \quad \text{for } m=1...3 \tag{21}$$

where ${}^me_j$ denotes the coordinates of a unit direction vector for principal strain direction m. Since the principal frame of the total macroscopic strain tensor is used, the unit vectors have the following coordinates:

$${}^1e_j = (1,0,0),\ {}^2e_j = (0,1,0),\ {}^3e_j = (0,0,1) \tag{22}$$

The remaining equations are obtained by enforcing equilibrium between the tractions on the other surfaces of the band and the elastic spring;

$$\sigma_{ij}^b\,{}^me_j = {}^n\sigma_{ij}^u\,{}^me_j \tag{23}$$

where m 1..3, n 1...3, m n

It should be noted that this is different from the one-dimensional localization element where the kinematic constraint (12) was used for these surfaces. The equation (23) is equivalent to a static con-

straint on the remaining stress and strain components of the elastic springs. Formulas (21) and (23) together with the assumption of stress tensor symmetry represent the remaining 18 equations that are needed for the solution of the three-dimensional equivalent localization element. These 18 equations can be written as:

$$\sigma_{ij}^{b} = {}^{m}\sigma_{ij}^{u} \quad \text{for} \quad m = 1...3 \qquad (24)$$

This means that the macroscopic stress must be equal to σ_{ij}^{b}, i.e. stress in the localization element, and that the stresses in all three elastic springs must be equal to each other and to the microplane stress σ_{ij}^{b}. This implies also the equivalence of all three elastic strain tensors.

The resulting system of non-linear equations is again solved by Newton-Raphson iterations (Cervenka et. al. (2001).).

The macroscopic stress is then equal to the stress in the localization band σ_{ij}^{b}. Contrary to the one-dimensional localization element there are no restrictions. All the types of localization modes and all the directions of failure propagation can be considered.

6 EXAMPLES OF APPLICATION

This section demonstrates the application of the presented method on three example problems. The goal is to investigate the objectivity of results with respect to the element size when the equivalent crack band localization element is used. The finite element method is employed, and always several element sizes are used to demonstrate the mesh size objectivity. The same example problems and the same meshes are also calculated with the microplane model without the equivalent crack band approach. This comparison should clearly show the benefits of the proposed approach. All examples presented in this paper are calculated by the program ATENA. ATENA is an implicit code based on the finite element method incorporating modern numerical techniques such as for instance: the object oriented approach and template meta-programming.

6.1 *A single large element in tension*

The first example is a uni-axial tension problem. The geometry of the problem corresponds to the tension specimens tested by Hordijk (1991). Three specimens were analyzed, with the same cross-sectional area but with different lengths. The dimensions and geometry are shown in Table 1 and Figure 4, respectively.

Table 1: Specimen dimensions

Specimen	Length [mm]	Width [mm]	Height [mm]
A	250	50	50
B	125	50	50
C	50	50	50

When large finite elements are used in a finite element calculation that is dominated by a tensile failure, each element should correctly reproduce the macroscopic behavior of a tensile experiment. For this reason, every specimen is modeled by only one finite element with a different length. Each case should reproduce the macroscopic behavior of the corresponding uni-axial tension test.

All the specimens are loaded by prescribed deformations, and the reaction forces are monitored during the analysis.

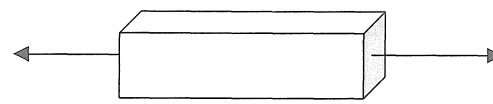

Figure 4. Tensile specimen geometry and loading

The results of numerical analysis are compared with the experiment of Hordijk (1991). In the experiment the following material properties of concrete were measured: the modulus of elasticity E=18000 MPa, cubic compresive strength f_{cu} =-50.4 MPa, direct tensile strength f_t = 3.3 MPa, and maximal aggregate size d_{max}=2 mm. The default material parameters of the microplane model are used in the analysis (k_2=500,k_3=15,k_4=150, as defined in Bažant et al. 2000a) with the exception of the microplane parameter k_1 that was determined by fitting the experimental tensile strength

Two finite element analyses are performed for each geometry: one with the equivalent crack band model and one without it. The crack band size h is set to $1.5\,d_{max}$, where d_{max} is the aggregate size, i.e. $h = 3$ mm. Figure 5 shows the obtained stress-deformation relations for all specimens; the label "band" indicates the analyses in which the equivalent crack band element (ECBE) method is used. The curves without this label are calculated by the standard microplane model. The L means the length of the specimen. The deformation corresponds to the crack opening displacements. The figure shows that the specimens failed at the same tensile stress level. The computed data are compared with the measured data from the experiment by Hordijk (1991). This figure clearly shows the benefit of the proposed method. It can correctly reproduce the crack opening law, independently of the finite element size. This is in sharp contrast to the results from the plain use of the microplane model, in which a strong dependence on the finite element size is observed.

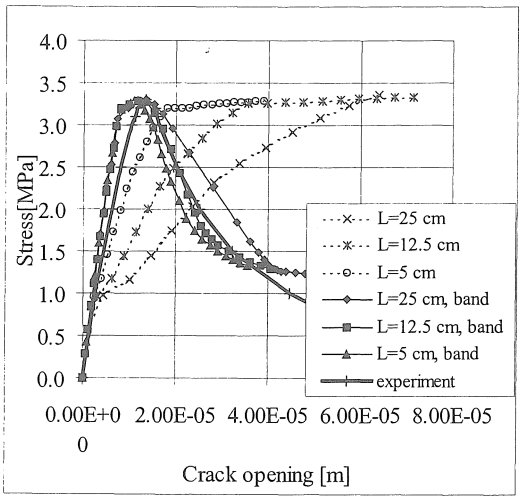

Figure 5. Diagrams of stress versus crack opening displacement from the tension test.

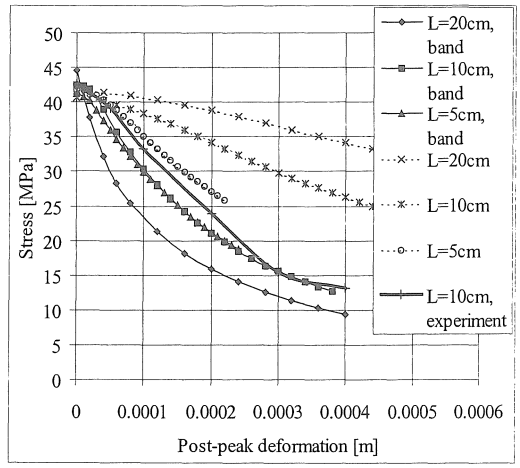

Figure 6: Diagrams of stress versus post-peak displacement $u = u_{tot} - u_{peak}$.

6.2 *A single large element in compression*

The second example problem is similar to the first one, but this time a compressive behavior is considered. Prisms with square cross-section and with different length are analyzed using a single finite element. Each analysis should be able to reproduce the behavior of a similar experiment. This time the experimental data by van Mier (1986) are used for comparison. Table 2 shows the important dimensions of the tested specimens.

Table 2: Dimensions of compressive specimens

Specimen	Length [mm]	Width [mm]	Height [mm]
A	50	100	100
B	100	100	100
C	200	100	100

In the experimental work the following basic material properties are reported: the elastic modulus E=28 000 MPa, cubic strength f_{cu}=42.6 MPa, maximal aggregate size d_{max}=16 mm. The default material parameters of the microplane model are again used in the analysis (k_2=500,k_3=15,k_4=150) with the exception of the microplane parameter k_1 that was determined by fitting the experimental compressive strength. The final value of this parameter is set to $k_1=1.72\times10^{-4}$.

These specimens are loaded by prescribed deformations, and the reaction forces are monitored and used for the stress calculation. Again the numerical model is formed by a single finite element. Two analyses are performed for each length: one with the ECBE method and one without it. In the ECBE method, two crack band sizes are used. For directions parallel with the negative principal strain direction $b^- = 3\,d_{\max} = 48$ mm, and for positive principal strains $b^+ = 1.5\,d_{\max} = 24$ mm. Figure 6 demonstrates the effect that was documented by van Mier (1986). It was observed that if the peak deformation is subtracted from the total deformation, the obtained post-peak curves are quite independent of the specimen length. This experimental observation is well reproduced by the ECBE method.

6.3 *The shear beam of Leonhardt and Walther*

This example shows a simply supported reinforced concrete beam without shear reinforcement. An effect of the finite element mesh and crack band size on the shear failure of the beam is investigated. The geometry, loading, material properties and results are obtained from the work of Leonhardt & Walther (1962). The dimensions are depicted in Figure 7. The measured material properties of concrete were the modulus of elasticity E = 31 720 MPa and the cylindrical uni-axial compressive strength $f_c' = -8.5$ MPa. The steel properties were the modulus of elasticity E = 210 000 MPa and the yield stress f_y = 400 MPa. The same default material parameters of the microplane model were used as in the previous sections (k_2=500,k_3=15,k_4=150), with the exception of parameter k_1 that was determined by fitting the peak load.

The finite element models, shown in Figure 8, take advantage of the symmetry. The fine mesh has twelve elements along the height, the middle mesh six elements, the coarse mesh four elements. The

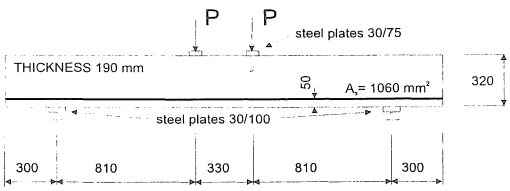

Figure 7: Geometry of Leonhardt and Walther's reinforced concrete beam.

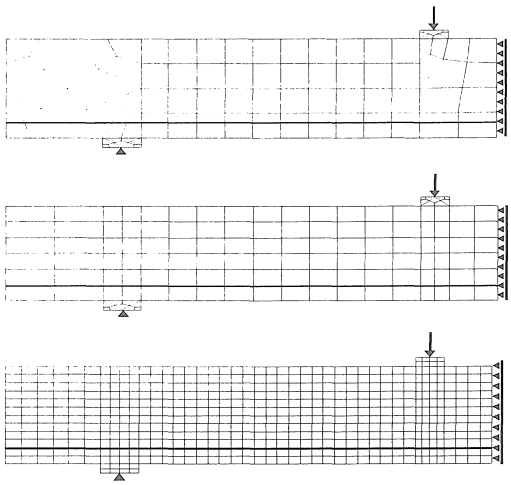

Figure 8. Meshes for the shear beam analysis.

computational model is loaded by prescribed deformations, and the reaction forces are monitored. For each mesh, two analyses are performed: one without and one with ECBE. The crack band size is set to $h = 25$ mm.. The calculated results without and with ECBE are shown in Figure 9.

The load-deflection diagrams again demonstrate the applicability of the proposed equivalent crack band element for the practical calculations. The diagrams calculated by the ECBE method are less sensitive to element size, and they very well predict the peak load. It may be mentioned that the analyses have again been performed using the default material parameters, with minimal fitting.

7 CONCLUSIONS

This paper presents a novel method for the implementation of softening material models defined by stress-strain relationships into finite element calculations with variable and large element sizes. The only additional parameter is the size h of the localization band. This size physically represents the characteristic dimension of the material for which the material formulation is calibrated. The underly-

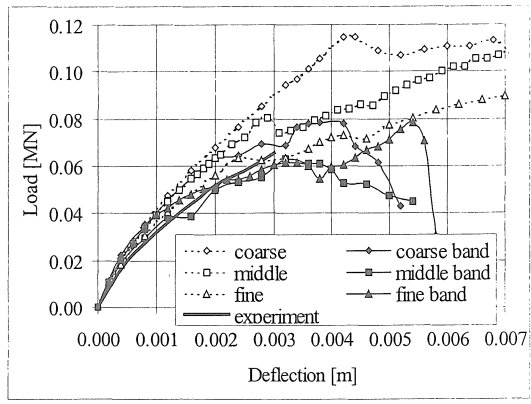

Figure 9: The load-deflection relation for the shear beam with ECBE (crack band size h=25mm)

ing assumption is that only one localization zone develops in a single finite element. The presented approach allows the use of different sizes h for each direction. In the current implementation, the spring directions are aligned with the principal strain directions, and two values of h are used: $h = 1.5\, d_{\max}$ for directions with positive principal strain and $h = 3\, d_{\max}$ for directions with negative principal strain. The different values of h are introduced to differentiate between the tensile fracturing and compressive crushing.

The disadvantage of the proposed method is the necessity to evaluate the microplane model several times, which increases the computational time. Typically, about 8 iterations are needed.

The proposed approach is demonstrated using the microplane model of Bažant et. al. (2000a), but is suitable for other material models as well. It can eliminate the mesh size sensitivity of strain softening material models.

The sensitivity of finite element calculations to mesh orientation cannot be addressed by this approach. It can be alleviated only by some non-local techniques.

The proposed method, however, could be used to supplement non-local concepts so as to eliminate the need for using very small finite elements. With the proposed method, the averaging volume in the non-local concept does not have to be fixed, but it can depend on the finite element size, such that the number of elements lying within the averaging volume (probably at least 3 to 4 in 2D analysis) would suffice to eliminate the mesh orientation bias.

ACKNOWLEDGMENTS

Partial financial supports for the first author and for the Visiting Scholar appointment of the second author at Northwestern University under U.S. National Science Foundation Grants CMS-9732791 and INT-9531299 are gratefully appreciated. The second and third authors would like to thank Czech Grant Agency for supporting this research under contract 103/99/0755.

REFERENCES

Bažant, Z.P., and Oh, B.H. 1983. Crack band theory for fracture of concrete, *Materials and Structures, RILEM*, Paris, France, 16, p. 155-177.

Bažant, Z.P. 1984. Microplane model for strain controlled inelastic behavior, Chapter 3 in *Mechanics of Engineering Materials* (Proc., Conf. held at U. of Arizona, Tucson, Jan. 1984), C.S. Desai and R.H. Gallagher, eds., J. Willey, London, 45-59.

Bažant, Z.P., Caner, F.C, Carol, I., Adley, M.D., and Akers, S.A. 2000a. Microplane model M4 for concrete: I. Formulation with work-conjugate deviatoric stress, *J. of Engrg. Mechanics ASCE* 126 (9), 944—953.

Caner, F.C., and Bažant, Z.P. 2000b. "Microplane model M4 for concrete: II. Algorithm and calibration.", *J. of Engrg. Mechanics ASCE* 126 (9), 954—961.

Červenka, J., Bažant, Z.P and Wierer, M.. (2001). Equivalent Localization Element for Crack Band Approach to Mesh-sensitivity in Microplane Model. *Int. Journal of Numer. Meth. Eng., submitted Spring 2001.*

ATENA 2000. *Program Documentation*, Červenka Consulting, www.cervenka.cz

Hordijk, D.A. 1991. Local approach to fatigue of concrete, T*heses Technische Universiteit Delft,* W.D. Meinema b. v. Delft, p. 47.

van Mier, J.G.M. 1986. Fracture of concrete under complex stress, *HERON,* Delft, Netherlands, 3, p.23.

Uchida, Y., Kurihara, N., Rokugo, K., and Koyanagi, W. 1995. Determination of tension softening diagrams of various kinds of concrete by means of numerical analysis, *Fracture mechanics of concrete structures,* AEDIFICATIO Publishers, Freiburg, p.25.